Astronomy & Astrophysics manuscript no. lpodio_ions_astroph
February 12, 2014
©ESO 2014

Molecular ions in the protostellar shock L1157-B1

L. Podio[1,2], B. Lefloch[1], C. Ceccarelli[1], C. Codella[2], and R. Bachiller[3]

[1] Institut de Planétologie et d'Astrophysique de Grenoble, 414, Rue de la Piscine, 38400 St-Martin d'Hères, France
e-mail: lpodio@arcetri.astro.it
[2] INAF - Osservatorio Astrofisico di Arcetri, Largo E. Fermi 5, 50125 Firenze, Italy
[3] IGN Observatorio Astronómico Nacional, Apartado 1143, 28800 Alcalá de Henares, Spain

Received ; accepted

arXiv:1402.2329v1 [astro-ph.GA] 10 Feb 2014

ABSTRACT

Aims. In this work, we perform a complete census of molecular ions with an abundance larger than $\sim 10^{-10}$ in the protostellar shock L1157-B1. This allows us to study the ionization structure and chemistry of the shock.
Methods. An unbiased high-sensitivity survey of L1157-B1 performed with the IRAM-30m and *Herschel*/HIFI as part of the CHESS and ASAI large programs allows searching for molecular ions emission. Then, by means of a radiative transfer code in the Large Velocity Gradient approximation, the gas physical conditions and fractional abundances of molecular ions are derived. The latter are compared with estimates of steady-state abundances in the cloud and their evolution in the shock calculated with the chemical model Astrochem.
Results. We detect emission from HCO^+, $H^{13}CO^+$, N_2H^+, HCS^+, and, for the first time in a shock, from $HOCO^+$, and SO^+. The bulk of the emission peaks at blueshifted velocity, $\sim 0.5-3$ km s^{-1} with respect to systemic, has a width of $\sim 4-8$ km s^{-1} and is associated with the outflow cavities ($T_{kin} \sim 20-70$ K, $n_{H_2} \sim 10^5$ cm^{-3}). A high velocity component, up to -40 km s^{-1}, associated with the primary jet is detected in the HCO^+ 1–0 line. Observed HCO^+ and N_2H^+ abundances ($X_{HCO^+} \sim 0.7-3\ 10^{-8}$, $X_{N_2H^+} \sim 0.4-8\ 10^{-9}$) are in agreement with steady-state abundances in the cloud and with their evolution in the compressed and heated gas in the shock for cosmic rays ionization rate $\zeta = 3\ 10^{-16}$ s^{-1}. $HOCO^+$, SO^+, and HCS^+ observed abundances ($X_{HOCO^+} \sim 10^{-9}$, $X_{SO^+} \sim 8\ 10^{-10}$, $X_{HCS^+} \sim 3-7\ 10^{-10}$), instead, are 1–2 orders of magnitude larger than predicted in the cloud; on the other hand they are strongly enhanced on timescales shorter than the shock age (∼2000 years) if CO_2, S or H_2S, and OCS are sputtered off the dust grains in the shock.
Conclusions. The performed analysis indicates that HCO^+ and N_2H^+ are a fossil record of pre-shock gas in the outflow cavity, while $HOCO^+$, SO^+, and HCS^+ are effective shock tracers and can be used to infer the amount of CO_2 and sulphur-bearing species released from dust mantles in the shock. The observed HCS^+ (and CS) abundance indicates that OCS should be one of the main sulphur carrier on grain mantles. However, the OCS abundance required to fit the observations is 1–2 orders of magnitude larger than observed. Laboratory experiments are required to measure the reactions rates involving these species and to fully understand the chemistry of sulphur-bearing species.

Key words. Stars: formation – ISM: jets & outflows – ISM: molecules – ISM: abundances – Astrochemistry

1. Introduction

The gravitational infall from which a new star is formed is accompanied by the ejection of highly supersonic jets. The shocks produced when the ejected material impacts on the high-density surrounding medium rapidly heat and compress the gas triggering several microscopic processes such as molecular dissociation, gas ionization, endothermic chemical reactions, ice sublimation, and dust grain disruption. It is well know that these processes produce a significant enhancement of the abundance of molecules which are evaporated or sputtered from dust grains, such as H_2CO, CH_3OH, NH_3, SiO (see, e.g., Bachiller & Perez Gutierrez 1997).

Molecular ions are commonly observed in dense prestellar/protostellar regions (e.g., Caselli et al. 1998, 2002; Hogerheijde et al. 1998) and their chemistry have been studied by means of gas-phase chemical models (e.g., Herbst & Leung 1986; Turner et al. 1999). In contrast, there are very few observations of molecular ions in protostellar shocks. HCO^+ was detected in a number of outflows and in some cases show a 'butterfly' morphology suggesting excitation in the outflow cavities (e.g., Hogerheijde et al. 1998; Girart et al. 1999, 2002; Lee et al. 2007; Tafalla et al. 2010; Tappe et al. 2012). Besides HCO^+, emission in HCS^+ and very recently in N_2H^+ lines was detected in the B1 shock along the chemically rich L1157 outflow (Bachiller & Perez Gutierrez 1997; Yamaguchi et al. 2012; Codella et al. 2013).

Due to the lack of observations, the chemical evolution of molecular ions in shocks has been poorly investigated. On the one hand, molecular ions are expected to be rapidly destroyed by electronic recombination in shocks; on the other hand, they may be enhanced due to the sputtering of dust grains mantles, which injects molecules in the gas phase where they undergo reactions leading to ions (e.g., Neufeld & Dalgarno 1989; Viti et al. 2002; Rawlings et al. 2004). Among the molecular ions previously observed in shocks, not all of them are due to changes caused by the shock itself. Codella et al. (2013) show that the N_2H^+ abundance is expected to decrease in shocks, hence the emission detected in the L1157-B1 shock is a probe of pre-shock chemistry. Molecular ions such as $HOCO^+$ and SO^+, instead, are believed to be effective tracers of shocked gas, as their abundance is predicted to be very low in the quiescent gas ($\leq 10^{-10}$) but could be strongly enhanced in shocks following the release of CO_2 and S-bearing molecules from dust grains mantles (e.g., Minh et al.

1991; Turner 1992, 1994; Deguchi et al. 2006). However, there are no observations of $HOCO^+$ and SO^+ undoubtedly associated with shocks.

In this paper, for the first time a complete census of molecular ions in a shock is given. This is obtained by means of a highly-sensitive unbiased spectral survey of the prototypical protostellar bow-shock L1157-B1 in the millimeter and submillimeter range, executed with the IRAM-30m telescope as part of the ASAI Large Program[1] (Astrochemical Surveys At Iram, Lefloch, Bachiller et al. in preparation) and with *Herschel*/HIFI as part of the Guaranteed Time Key Project CHESS[2] (Chemical HErschel Surveys of Star forming regions, Ceccarelli & CHESS Consortium 2010). The observations are presented in Sect. 2, while Sect. 3 summarizes the main properties of the L1157 outflow and the B1 bow-shock. In Sect. 4 we analyze the line profiles of the detected molecular ions and we perform a Large Velocity Gradient (LVG) analysis to infer the physical conditions of the emitting gas, and the abundance of molecular ions. Finally, in Sect. 5 we compare the observed abundances with steady-state abundances in the cloud and their evolution in the shock computed using the chemical code Astrochem. This allows us to distinguish between molecular ions which are tracing pre-shock chemistry, and those which are a useful probe of the shock properties and chemistry. Our conclusions are summarized in Sect. 6.

2. Observations and data reduction

2.1. IRAM-30m observations

The millimeter observations of L1157-B1 were acquired with the IRAM-30m telescope at Pico Veleta (Spain), as part of the ASAI Large Program (Lefloch, Bachiller et al. in preparation). The observed position in B1 is at $\alpha_{J2000} = 20^h\,39^m\,10\overset{s}{.}2$, $\delta_{J2000} = +68^\circ\,01'\,10\overset{''}{.}5$. The survey, obtained during several runs in 2011 and 2012, covers the spectral bands at 3 mm (80–116 GHz), 2 mm (128–173 GHz), 1.3 mm (200–320 GHz), and 0.8 mm (328–350 GHz). The observations were carried out in Wobbler Switching Mode, with a throw of 3′, and using the broad-band EMIR receivers and the FTS spectrometers in its 200 kHz resolution mode, corresponding to velocity resolutions of 0.17–0.75 km s^{-1}. The Half Power Beam Width (HPBW) varies between 7″ at 350 GHz and 31″ at 80 GHz. The data were processed using GILDAS/CLASS90[3] software. The spectra were smoothed by a factor of two, baseline subtracted and further resampled at lower spectral resolution if needed to increase the signal-to-noise. The rms achieved is typically 1.5 mK per interval of 0.4 MHz (i.e. $\sim$ 1.4 km s^{-1}) across the 3 mm band, and $\sim$ 5 mK per interval of $\sim$ 1 km s^{-1} in the 2 mm and 1.3 mm band. Line intensities are expressed in units of main-beam temperature, T_{mb}. We adopted the main-beam efficiencies, η_{mb}, monitored by IRAM (http://www.iram.fr). These decrease from 0.82 at 80 GHz to 0.33 in the sub-mm range.

2.2. Herschel/HIFI observations

The IRAM-30m survey is complemented by observations in the sub-millimeter range taken with the Heterodyne Instrument for the Far Infrared (HIFI, de Graauw et al. 2010) on board the *Herschel* Space Observatory[4] (Pilbratt et al. 2010) as part of the Guaranteed Time Key Project CHESS (Ceccarelli & CHESS Consortium 2010). The observations were carried out during 2010 towards the nominal position of B1 and in dual beam switch spectral scanning mode to cover most of the submillimeter bands 1 and 2 (488–628 GHz, 642–794 GHz). Both polarizations (H and V) were observed simultaneously. The receiver was tuned in double sideband (DSB) and the Wide Band Spectrometer (WBS) was used, providing a spectral resolution of 1.1 MHz, corresponding to 0.5–0.7 km s^{-1}, which was subsequently degraded to increase the sensitivity. The data were processed with the ESA-supported package Herschel Interactive Processing Environment[5] (HIPE, Ott 2010) version 6 package. Then level 2 fits files were transformed into GILDAS format for baseline subtraction and subsequent sideband deconvolution. The relative calibration between both receivers (H and V) was found very good, and the signals were co-added to improve the signal-to-noise. Line intensities were converted from antenna temperature, T_a, to main-beam brightness temperature, T_{mb}, using the main-beam efficiency, η_{mb}, as determined by Roelfsema et al. (2012).

3. Previous work on L1157

The L1157 outflow, located at a distance of $\sim$ 250 pc (Looney et al. 2007) and driven by the low mass Class 0 protostar L1157-mm ($\sim$ 4 $L_\odot$), is the most chemically rich outflow known so far (e.g., Bachiller & Perez Gutierrez 1997; Bachiller et al. 2001). Observations in CO, H_2, and H_2O lines reveal a highly collimated and precessing bipolar outflow (Davis & Eisloeffel 1995; Gueth et al. 1996), associated with several blue-shifted (B0, B1, B2) and red-shifted (R0, R1, R, R2) bow-shocks (Bachiller et al. 2001; Nisini et al. 2010) (see top panel of Fig. 1). Spectral surveys also revealed emission in molecules which are released from dust mantles, such as SO, H_2S, OCS, H_2CO, CH_3OH, H_2O, and NH_3 (Tafalla & Bachiller 1995; Bachiller & Perez Gutierrez 1997; Benedettini et al. 2007; Codella et al. 2010; Vasta et al. 2012), or sputtered from their core, such as SiO (Gueth et al. 1998; Nisini et al. 2007).

The brightest bow-shock B1 is an ideal laboratory to investigate the effect of shocks on gas chemistry because is located at $\sim$ 69″ from the protostar ($\sim$0.1 pc, see bottom panel of Fig. 1), hence UV irradiation can be neglected. The first results obtained from our IRAM-30m/*Herschel* survey further highlighted the chemical richness of B1 (Codella et al. 2010; Lefloch et al. 2010; Benedettini et al. 2012; Codella et al. 2012a,b, Busquet et al. submitted). High-angular resolution interferometric observations reveal that B1 has a clumpy structure with multiple components (Benedettini et al. 2007; Codella et al. 2009; Benedettini et al. 2013), which cannot be resolved by our single-dish IRAM-30m and *Herschel*/HIFI observations. However, Lefloch et al. (2012) showed that the analysis of the line profiles provides a simple tool to identify the different spatial and velocity components. In particular, the CO line profiles from J=1–0 to J=16–15 are well fit by a linear combination of three velocity components (g_1, g_2, and g_3), whose intensity-velocity relation follows an exponential law $I(V) = I(0)\exp(-|V/V_0|)$, with V_0 =

[1] http://www.oan.es/asai
[2] http://chess.obs.ujf-grenoble.fr
[3] http://www.iram.fr/IRAMFR/GILDAS

[4] *Herschel* is an ESA space observatory with science instruments provided by European-led Principal Investigator consortia and with important participation from NASA.
[5] HIPE is a joint development by the Herschel Science Ground Segment Consortium, consisting of ESA, the NASA Herschel Sci- ence Center, and the HIFI, PACS and SPIRE consortia.

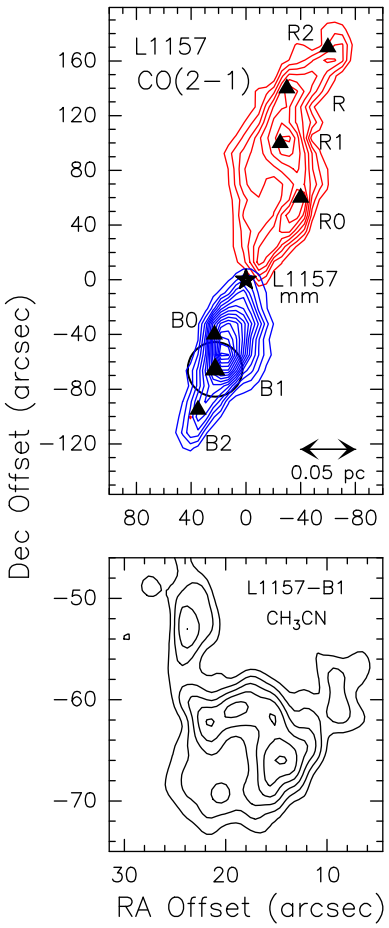

Fig. 1. *Top panel*: Integrated CO J=2–1 emission of the L1157 bipolar outflow (Bachiller et al. 2001). Offsets are with respect to the driving source L1157-mm (black star), at coordinates: α_{J2000} = 20^h 39^m 06^s.2, δ_{J2000} = +68° 02′ 16″.0. The black triangles and labels indicate the main blue- and red-shifted knots as defined by Bachiller et al. (2001). Circle is for the largest HPBW of the present dataset (40″), centred on the L1157-B1 bow-shock. *Bottom panel*: The L1157-B1 bow-shock as traced by the CH_3CN J=8–7 K=0,1,2 emission at 3 mm, observed with the IRAM PdB interferometer (Codella et al. 2009).

12.5, 4.4, and 2.5 km s^{-1} for g_1, g_2 and g_3, respectively. These velocity components trace different regions in the B1 bow-shock, characterized by different sizes and physical conditions:
(i) g_1: the jet impact region against the cavity (∼ 7 – 10″) in the L1157-B1 bow-shock, with gas at T_{kin} ∼ 210 K, reaching velocities up to −40 km s^{-1};
(ii) g_2: the outflow cavity associated with B1, made of gas at T_{kin} ∼ 60 – 80 K, reaching velocities up to −20 km s^{-1};
(iii) g_3: the cavity associated with the older outflow shock L1157-B2, made of colder gas (T_{kin} ∼ 20 K) at slower velocities (≤ −10 km s^{-1}).
Besides the three components evidenced by the analysis of the CO line profiles, a forth hot and tenuous component (T_{kin} ∼ 1000 K, n_{H_2} ∼ 10^4 cm^{-3}) is detected in H_2O lines (Busquet et al., submitted).

Interestingly, L1157-B1 also shows emission in molecular ions, such as HCO^+, HCS^+, and N_2H^+ (Bachiller & Perez Gutierrez 1997; Codella et al. 2010; Yamaguchi et al. 2012; Codella et al. 2013) making it a unique target to investigate the chemistry of molecular ions in protostellar shocks.

4. Results

4.1. Line identification

The ions identified down to the 3σ level (∼ 5 mK in the 3 mm band) in L1157-B1 are: HCO^+, $H^{13}CO^+$, N_2H^+, $HOCO^+$, SO^+, and HCS^+. Thanks to the high-sensitivity of our survey, several transitions of each molecular species are detected, allowing high accuracy in the derivation of the physical conditions. $HOCO^+$ and SO^+ are observed for the first time in L1157-B1 and, more in general, in a protostellar shock.

The properties of the detected lines (transition, frequency, upper level energy), and their observational parameters (HPBW, rms noise, peak velocity and temperature, Full Width at Half Maximum (FWHM), and integrated intensity) are summarized in Table 1. The line spectra are shown in Figure 2. All the detected lines peak at blueshifted velocity, ∼ 0.5 – 3 km s^{-1} with respect to systemic, and have a line width of ∼ 3–7 km s^{-1} which is consistent with emission originating in the outflow cavities B1 and B2. A detailed analysis of the observed line profiles for each molecular ion is presented in the following sections.

4.2. Physical conditions and abundances

The gas physical conditions and the column density and abundance of each molecular species were derived from a multi transition analysis, by means of a radiative transfer code in the LVG approximation whenever more than one line is detected and the collisional coefficients are available (HCO^+, $HOCO^+$, and HCS^+), and in the hypothesis of Local Termodinamic Equilibrium (LTE) otherwise (N_2H^+, and SO^+). The Einstein coefficients and upper level energies are retrieved from the Jet Propulsion Laboratory (JPL) database[6] (Pickett et al. 1998) and the Cologne Database of Molecular Spectroscopy (CDMS)[7] (Müller et al. 2001), while the collisional coefficients are taken from the BASECOL database[8] (Dubernet et al. 2013). In particular, the reference for the collisional coefficients are: Flower (1999) for HCO^+; Hammami et al. (2007) for $HOCO^+$; Monteiro (1984) for HCS^+. In the case in which an LTE analysis is applied the main source of uncertainty on the derived abundance is the assumed excitation temperature and size of the emitting region. This leads to an uncertainty of up to an order of magnitude for N_2H^+, and about a factor three for SO^+, for which the excitation temperature is derived by fitting the detected transitions. When, instead, an LVG analysis is applied the uncertainty on the abundance is obtained by considering the difference between the best-fit and the second best-fit solutions and is around a factor three. The gas kinetic temperature and H_2 density, T_{kin} and n_{H_2}, the column density, $N_{species}$, and fractional abundances with respect to H_2, $X_{species}$, derived for the analysed molecular ions are summarized in Tab. 2.

4.2.1. HCO^+ and isotopologues

Figs. 2a and 2d show all the detected transition from HCO^+ and its isotopologue $H^{13}CO^+$. HCO^+ has been widely detected in prestellar cores (e.g., Caselli et al. 1998), in embedded low-mass protostars, and along their outflows (e.g., Hogerheijde et al. 1998). HCO^+ emission is detected up to the J = 7–6 transition. We also detect emission from $H^{13}CO^+$ in the 1–0 and, tentatively, in the 3–2 line (the latter with a signal-to-noise

[6] http://spec.jpl.nasa.gov
[7] http://www.astro.uni-koeln.de/cdms
[8] http://basecol.obspm.fr/

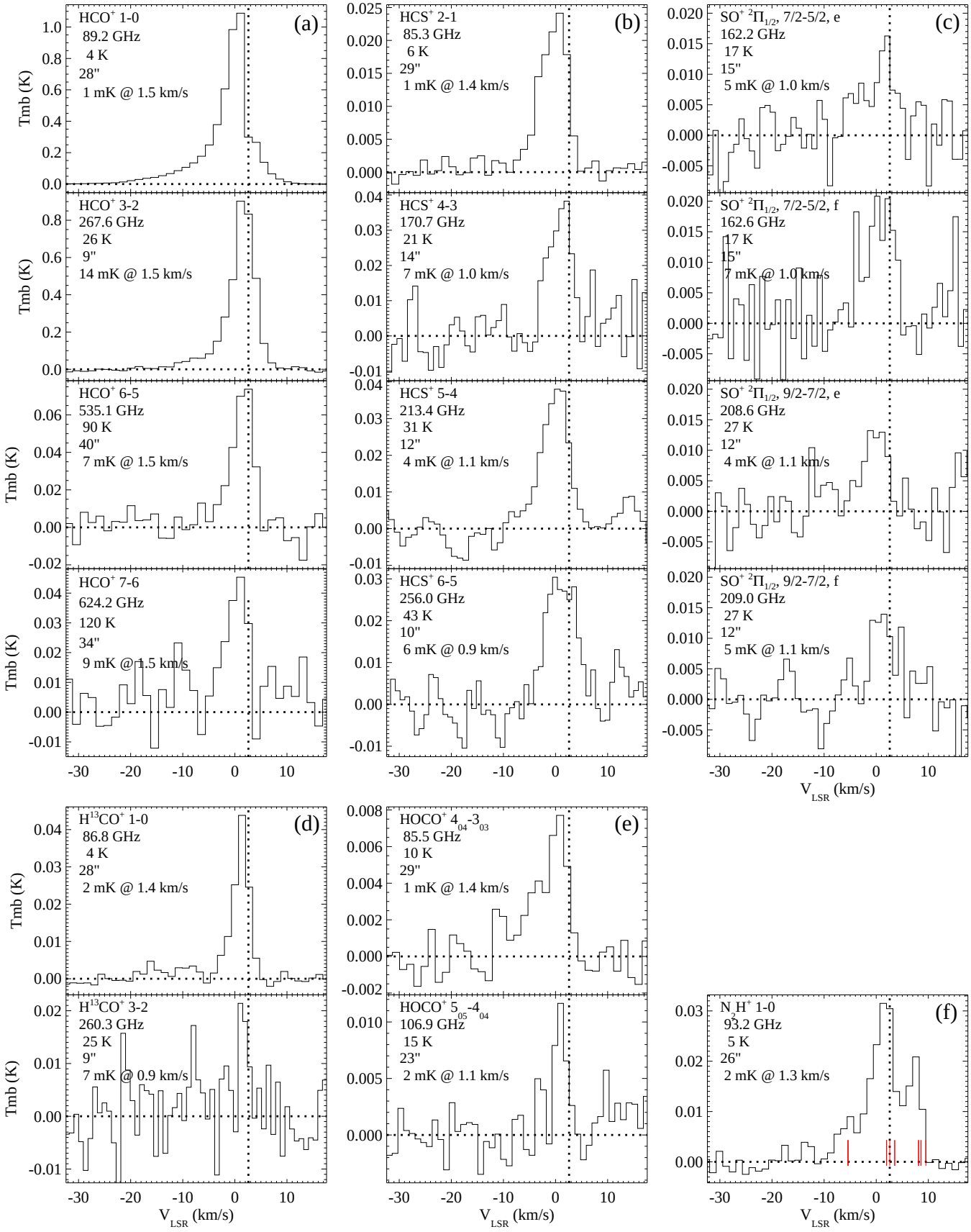

Fig. 2. Line profiles of the molecular ions observed in the L1157-B1 shock: HCO^+ (a), HCS^+ (b), SO^+ (c), $H^{13}CO^+$ (d), $HOCO^+$ (e), N_2H^+ (f). The line intensity is in mean beam temperature (T_{mb}). The transition, frequency in GHz, upper level energy in K, HPBW in arcsec, and 1σ rms noise in mK are indicated. The baseline and the systemic velocity (V_{LSR} = +2.6 km s^{-1}) are indicated by the horizonthal and vertical dotted lines. For N_2H^+ (f) the 15 hyperfine components of the N_2H^+ 1–0 pattern are indicated by the vertical red lines (due to degeneracy only 7 of the 15 hyperfine lines do not overlap in frequency; of these, only the three main groups are resolved because of blending caused by the line broadening).

Table 1. Properties of the detected lines from molecular ions: species, transition, frequency (ν_0, in MHz), upper level energy (E_{up}, in K), telescope Half Power Beam Width (HPBW, in arcseconds), rms noise (in mK), peak velocity (V_{peak}, in km s^{-1}) and temperature (T_{peak}, in main-beam temperature units), full width at half maximum (FWHM, in km s^{-1}) and integrated intensity ($\int T_{mb}dV$, in K km s^{-1}). All transitions are observed with IRAM-30m/FTS, except those indicated by the star which are observed with *Herschel*/HIFI. A gaussian fit is applied to estimate the line properties for most of the transitions. When the line profile is non-gaussian the line intensity is obtained by integrating the area below the profile. For each species we report a 3σ upper limit for the first non-detected transition covered by our observations.

Species	Transition	ν_0[a]	E_{up}	HPBW	rms	V_{peak}	FWHM	T_{peak}	$\int T_{mb}dV$
		MHz	K	$''$	mK	km s^{-1}	km s^{-1}	mK	K km s^{-1}
HCO^+	J = 1–0[ng]	89 188.52	4	28	1	1.1 ± 1.5	4.4 ± 1.5	1095 ± 1	7.40 ± 0.01
	J = 3–2[ng]	267 557.53	26	9	14	1.2 ± 1.5	6.0 ± 1.5	901 ± 14	5.49 ± 0.09
	J = 6–5*	535 061.38	90	40	7	1.6 ± 0.2	4.6 ± 0.4	76 ± 7	0.38 ± 0.03
	J = 7–6*	624 208.19	120	34	9	0.5 ± 0.4	3.5 ± 0.8	37 ± 9	0.14 ± 0.03
	J = 8–7*	713 342.12	154	30	35	-	-	-	≤ 0.29
$H^{13}CO^+$	J = 1–0	86 754.29	4	28	2	1.2 ± 0.1	3.7 ± 0.2	39 ± 2	0.15 ± 0.00
	J = 3–2	260 255.34	25	9	7	1.6 ± 0.3	1.8 ± 0.7	23 ± 7	0.04 ± 0.01
	J = 4–3	346 998.34	42	7	29	-	-	-	≤ 0.16
N_2H^+[b]	J = 1–0	93 173.76	5	26	2	1.3 ± 0.1	4.3 ± 0.2	29 ± 2	0.33±0.01
	J = 3–2	279 511.83	27	9	5	-	-	-	≤ 0.03
$HOCO^+$[c]	$J_{K_{-1}K_1} = 4_{04}$–3_{03}[ng]	85 531.51	10	29	1	0.9 ± 1.4	6.8 ± 1.4	8 ± 1	0.06 ± 0.01
	$J_{K_{-1}K_1} = 5_{05}$–4_{04}[ng]	106 913.57	15	23	2	1.0 ± 1.1	3.3 ± 1.1	12 ± 2	0.04 ± 0.01
	$J_{K_{-1}K_1} = 6_{06}$–5_{05}	128 295.06	22	19	11	-	-	-	≤ 0.07
SO^+[d]	$^2\Pi_{1/2}$, J = 5/2–3/2, l = e	115 804.41	9	21	13	-	-	-	≤ 0.09
	$^2\Pi_{1/2}$, J = 5/2–3/2, l = f	116 179.95	9	21	15	-	-	-	≤ 0.12
	$^2\Pi_{1/2}$, J = 7/2–5/2, l = e[ng]	162 198.59	17	15	5	2.0 ± 1.0	2.9 ± 1.0	13 ± 5	0.09 ± 0.02
	$^2\Pi_{1/2}$, J = 7/2–5/2, l = f	162 574.06	17	15	7	0.6 ± 0.8	6.3 ± 1.5	17 ± 7	0.12 ± 0.03
	$^2\Pi_{1/2}$, J = 9/2–7/2, l = e	208 590.03	27	12	4	-0.2 ± 0.6	5.7 ± 1.7	13 ± 4	0.08 ± 0.02
	$^2\Pi_{1/2}$, J = 9/2–7/2, l = f	208 965.42	27	12	4	1.3 ± 0.7	5.6 ± 2.0	13 ± 4	0.08 ± 0.02
	$^2\Pi_{1/2}$, J = 11/2–9/2, l = e	254 977.94	39	10	5	-	-	-	≤ 0.03
	$^2\Pi_{1/2}$, J = 11/2–9/2, l = f	255 353.23	39	10	5	-	-	-	≤ 0.03
HCS^+	J = 2–1	85 347.90	6	29	1	-0.3 ± 0.8	6.2 ± 1.9	23 ± 1	0.15 ± 0.04
	J = 4–3	170 691.73	21	14	7	0.9 ± 0.3	5.6 ± 0.7	36 ± 7	0.21 ± 0.02
	J = 5–4	213 360.53	31	12	4	0.0 ± 0.2	6.2 ± 0.5	38 ± 4	0.25 ± 0.02
	J = 6–5	256 027.80	43	10	6	1.1 ± 0.3	6.9 ± 0.7	30 ± 6	0.22 ± 0.02
	J = 7–6	298 690.88	57	8	16	-	-	-	≤ 0.09

*observed with *Herschel*/HIFI.
[ng]non-gaussian profile. The line intensity is obtained by integrating the area below the profile.
[a]frequencies are from the JPL molecular database (Pickett et al. 1998), and from the CDMS database (Müller et al. 2001) for N_2H^+.
[b]the line properties quoted for the N_2H^+ 1–0 and 3–2 transitions refer to the brightest of their 15 and 45 hyperfine components, i.e. the F1, F = 2,3–1,2 and the F1, F = 4,5–3,4 components, respectively. The line intensity is integrated over all the components.
[c]the transitions of $HOCO^+$ are characterized by the quantum numbers J, which is the total angular momentum, and K_{-1}, K_1, which are the angular momenta around the molecule's symmetry axis.
[d]SO^+ is a reactive radical with $^2\Pi_{1/2}$ ground state, whose spin-doubled rotational transitions, characterized by the quantum number J, are further split by Λ-type doubling.

of 4). The $HC^{18}O^+$ 1–0, and 3–2 lines, instead, are not detected. The HCO^+ 1–0 line shows bright and very broad wings extending up to −40 km s^{-1}. So far, only CO, H_2O, and SiO have been observed at these extreme velocities in L1157-B1 (Lefloch et al. 2010, 2012). High-velocity emission in HCO^+ lines has been detected also in the outflows driven by the Class 0 protostars L1448-mm and IRAS 04166+2706 (Tafalla et al. 2010).

The HCO^+ 1–0 line optical depth is derived from the HCO^+ to the $H^{13}CO^+$ 1-0 line ratio assuming an isotopic ratio of 77 (Wilson & Rood 1994). A simple LTE analysis of the $^{12}C/^{13}C$ line ratio, R, indicates that the HCO^+ 1–0 emission is optically thick at the cloud velocity (R ∼ 11, $\tau \sim 7$) and becomes optically thin in the wings (R ∼ 68, $\tau \sim 0.3$ at ∼ −2 km s^{-1}).

We tentatively fit the profile of the HCO^+ 1–0 line using the three exponential components as for CO. A good fit is obtained adopting for the three components the zero velocity intensities summarized in Fig. 3. Similarly to what has been found for the CO lines (Lefloch et al. 2012), the bulk of the emission originate in the outflow cavity B1 (g_2), while the g_1 jet component is dominant at high velocities (V < −20 km s^{-1}), and the g_3 component, accounting for the emission from the old cavity B2, is contributing only close to systemic velocity. The emission excess detected between −20 km s^{-1} and −15 km s^{-1} could be related to the compact clumps along the cavity detected with high-resolution interferometric observations and showing a second emission peak at those velocities (Benedettini et al. 2013). The higher-J HCO^+ lines are detected with lower signal-to-noise, thus the g_1 component remains undetected and they are fit by a combination of the g_2 and g_3 components.

We use an LVG model to fit the fluxes of all the HCO^+ lines, after subtracting the g_1 component from the HCO^+ 1–0 line. The flux of the different lines is well accounted for by extended emis-

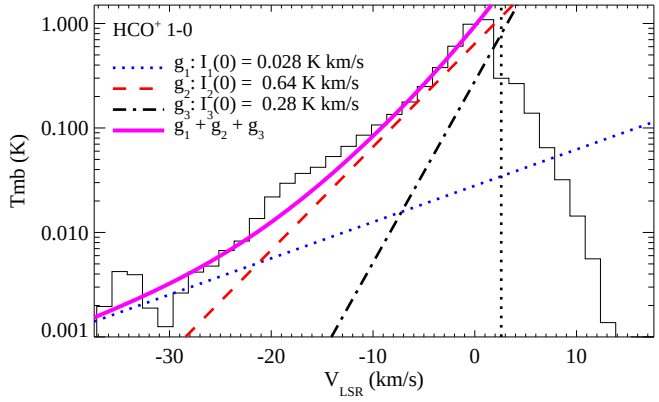

Fig. 3. Profile of the HCO^+ 1–0 line observed in the L1157-B1 shock. The line intensity is in mean beam temperature (T_{mb}) and the systemic velocity (V_{LSR} = +2.6 km s^{-1}) is indicated by the vertical dotted lines. The line profile is fit by a linear combination of three exponential functions g_1 = $I_1(0)$ exp(-|V/12.5 km/s|) (blue dotted line), g_2 = $I_2(0)$ exp(-|V/4.4 km/s|) (red dashed line), and g_3 = $I_3(0)$ exp(-|V/2.5 km/s)| (dotted-dashed black line). The (g_1 + g_2 + g_3) line fit is overplotted (magenta solid line).

sion from a single gas layer at T_{kin} ∼ 60 K, n_{H_2} ∼ 10^5 cm^{-3}, and a column density N_{HCO^+} ∼ 6 10^{12} cm^{-2}. This solution is in very good agreement with the size and physical conditions found for the outflow cavity B1 (g_2 component) for the CO lines (Lefloch et al. 2012) (see Table 2). Adopting the CO column density found by these authors, N_{CO} = 9 10^{16} cm^{-2}, we estimate an HCO^+ relative abundance $X_{HCO^+}(g_2) = N_{HCO^+}/N_{H_2} \sim 7\ 10^{-9}$.

A tentative estimate of the HCO^+ abundance in the jet component g_1, can be obtained by assuming the same physical conditions as for CO (T_{kin} = 210 K, $n_{H_2} \geq 10^6$ cm^{-3}) and computing the HCO^+ column density required to account for the g_1 integrated area. Adopting ΔV = 10 km s^{-1}, we estimate a column density N_{HCO^+} ∼ 1 − 3 10^{12} cm^{-2}, depending on the assumed density (n_{H_2}= $10^6 - 10^7$, respectively), implying an HCO^+ abundance $X_{HCO^+}(g_1)$ ∼ 1 − 3 10^{-8}. The abundance estimated in the g_1 component is in agreement within a factor of two with the estimate by Bachiller & Perez Gutierrez (1997). We recall that the latter is derived using only the 1–0 line and assuming that the emission is optically thin and thermalized (T_{kin} = 80 K).

Within the uncertainties of the present and previous studies by Bachiller & Perez Gutierrez (1997), the HCO^+ abundance estimated both in the jet impact region (g_1) and in the outflow cavities (g_2) can be considered in agreement with what estimated at the source position by Bachiller & Perez Gutierrez (1997) within a factor of a few. This is in agreement with previous observations of outflows in the HCO^+ lines showing no evident enhancement of the HCO^+ abundance both in the outflow cavities and in the high velocity component with respect to dense core value (Hogerheijde et al. 1998; Tafalla et al. 2010). The chemistry of HCO^+ and its evolution in the shock will be discussed in Sect. 5.

4.2.2. N_2H^+

A detailed analysis of the detected N_2H^+ 1–0 line (see Fig. 2f) is presented in Codella et al. (2013). These authors show that the observed line profile is consistent with emission by either the B1 outflow cavity (g_2) and/or with the older and colder B2 cavity (g_3). The peak velocity and line width (V_{peak} ∼ +1.3 km s^{-1}, FWHM ∼ 4.3 km s^{-1}) are in agreement with those found for the other molecular ions. The colum density and fractional abundance ($N_{N_2H^+}$ ∼ 0.4 − 8 10^{12} cm^{-2}, $X_{N_2H^+}$ ∼ 0.4 − 8 10^{-9}) are derived by assuming LTE conditions at a temperature of ∼ 20 − 70 K and an emitting size of ∼ 20 − 25″ as derived from the analysis of the CO lines by Lefloch et al. (2012). As for HCO^+, also N_2H^+ is not enhanced in the shock with respect to the on-source value estimated by Bachiller & Perez Gutierrez (1997). The chemistry of N_2H^+ is further discussed in Sect. 5.

4.2.3. $HOCO^+$

We detect $HOCO^+$ emission in the $4_{04} - 3_{03}$ and $5_{05} - 4_{04}$ lines at 85.5 and 106.9 GHz (see Fig. 2e). So far $HOCO^+$ has been detected in different environments, i.e. in the Galactic center region (Thaddeus et al. 1981; Minh et al. 1988, 1991; Deguchi et al. 2006), in translucent and dark clouds (Turner et al. 1999), and around the low-mass Class 0 protostar IRAS 04368+2557 in L1527 (Sakai et al. 2008). The reported detection, however, is the first one directly associated with a shock spot.

The signal-to-noise of the detected lines is quite low (∼ 4–6). Similarly to the other ions, the profiles favor an origin in the outflow cavities B1 and/or B2 (g_2, g_3). However, the lower excitation $HOCO^+$ $4_{04} - 3_{03}$ line at 85.5 GHz also shows a blueshifted wing extending up to −12 km s^{-1}. From an LVG analysis including the two detected lines and the upper limit for the $6_{06} - 5_{05}$ line at 128.3 GHz we find that the emission is extended and the best fit is obtained for n_{H_2} ∼ 10^4 cm^{-3}, T_{kin} ∼ 35 K, N_{HOCO^+} ∼ 10^{12} cm^{-2}. Thus, if we consider a CO column density of ∼ 10^{17} (g_2, g_3) we find X_{HOCO^+} ∼ 10^{-9}.

The estimated abundance is 1-2 orders of magnitude larger than what predicted by gas-phase chemistry in cold quiescent clouds (Herbst & Leung 1986; Turner et al. 1999). Previous studies suggest that $HOCO^+$ may be enhanced in shocks and/or UV irradiated regions due to the release of CO_2 from dust grain mantles, then reacting with H_3^+ to form $HOCO^+$ (Herbst et al. 1977; Minh et al. 1991; Deguchi et al. 2006; Sakai et al. 2008). However, those studies are based on unresolved observations of complex environments and do not allow to conclude on the origin of $HOCO^+$. Our detection in the L1157-B1 shock, located 69″ away from source, is a strong confirmation that $HOCO^+$ is an effective shock tracer. The chemistry $HOCO^+$ and the origin of the observed emission is further discussed in Sect. 5.

4.2.4. SO^+

Fig. 2c shows the SO^+ transitions detected by our IRAM-30m observations. Up to date SO^+ lines have been detected in the shocked molecular clump associated with the supernova remnant IC 443G (Turner 1992), in cold clouds and warm active star froming regions (Turner 1994), and in translucent molecular clouds (Turner 1996). The reported detection is the first detection of SO^+ emission directly associated with a protostellar shock. We could not detect the SO^+ doublet at 115.8, 116.2 GHz in the 3mm band (E_{up} ∼ 9 K) because of the high rms noise (about 13–15 mK). The lines from the higher excitation doublets at 162.2, 162.6 GHz (E_{up} ∼ 17 K), at 208.6, 209.0 GHz (E_{up} ∼ 27 K) are detected.

The line profiles suggest that they are dominated by emission from the outflow cavities (g_2, g_3) with no evidence of high velocity emission from the jet impact region (g_1). However, the emission is rather weak and the signal to noise ratio is not high enough to firmly conclude about the origin of the emission from a simple line profile analysis. Since no collisional coefficients

Table 2. Gas physical conditions (kinetic temperature, T_{kin}, and H_2 density, n_{H_2}), column density, $N_{species}$, and fractional abundances, $X = N_{species}/N_{H_2}$, for CO (Lefloch et al. 2012) and the observed molecular ions as derived from an LVG (for HCO^+, $HOCO^+$, and HCS^+) or LTE (for N_2H^+ and SO^+) analysis of the detected lines. The values derived for N_2H^+ are from Codella et al. (2013).

Species	Cmp	T_{kin} K	n_{H_2} cm^{-3}	$N_{species}$ cm^{-2}	$X = N_{species}/N_{H_2}$
CO[a]	g_1	210	$\geq 10^6$	$9\ 10^{15}$	10^{-4}
	g_2	60–80	$\geq 10^5$	$9\ 10^{16}$	10^{-4}
	g_3	20	$\geq 10^5$	$1\ 10^{17}$	10^{-4}
HCO^+	g_1	210[b]	10^6-10^{7}[b]	1–3 10^{12}	1–3 10^{-8}
	g_2	60	10^5	$6\ 10^{12}$	$7\ 10^{-9}$
N_2H^+[c]	g_2/g_3	20–70[c]	-	0.4–8 10^{12}	0.4–8 10^{-9}
$HOCO^+$	g_2/g_3	35	10^4	$1\ 10^{12}$	$1\ 10^{-9}$
SO^+[d]	g_2/g_3	25[d]	-	$7\ 10^{11}$	$8\ 10^{-10}$
HCS^+	g_2	80	$8\ 10^5$	$6\ 10^{11}$	$7\ 10^{-10}$
	g_3	20[e]	10^5[e]	$3\ 10^{11}$	$3\ 10^{-10}$

[a] Lefloch et al. (2012). The fractional abundance of CO is assumed
[b] T_{kin} and n_{H_2} in g_1 are assumed to be as derived from CO
[c] $N_{N_2H^+}$, $X_{N_2H^+}$ estimated by Codella et al. (2013) assuming LTE at T_{kin} = 20 − 70 K and a source size of ∼ 20 − 25″ as inferred from CO
[d] Since no collisional coefficients are available we apply an LTE analysis assuming that the emission originates in the extended outflow cavities (g_2, g_3). Hence, at difference with the other ions, the estimated temperature is an excitation temperature, T_{ex}
[e] T_{kin} and n_{H_2} in g_3 are assumed to be as derived from CO. This assumption relies on the similarity of CO and HCS^+ profiles at low velocities and on the results of the LVG analysis (see text).

are available, we derive the SO^+ abundance from the detected line fluxes under the hypothesis of LTE. The SO^+ abundance estimated under this hypothesis depends on the size of the emitting region, thus we consider two limiting-cases.

If we assume that SO^+ arises from the outflow cavities, either B1 (g_2) or B2 (g_3), the emission is more extended than the beam size, and, as first order, the main-beam brightness temperature is a reasonable approximation of the intrinsic source brightness temperature. The relative intensities of the doublets at 162 GHz and 208 GHz imply an excitation temperature of ∼ 25 K; we estimate a column density $N_{SO^+} \sim 7\ 10^{11}$ cm^{-2} and a relative abundance $X_{SO^+} \sim 8\ 10^{-10}$.

If instead we assume that SO^+ originates from the compact jet impact region ($g_1 \sim 7 - 10''$), then one has to correct for the source coupling with the telescope beam. We estimate the source coupling factor from an SiO J=8–7 map at 7.4″ resolution obtained at the IRAM-30m telescope, convolved at the resolution of the different SO^+ transitions. Our LTE analysis then yields $T_{ex} \sim 10$ K and a column density $N_{SO^+} \sim 2\ 10^{12}$ cm^{-2}, corresponding to a relative abundance $X_{SO^+} \sim 2\ 10^{-8}$. The derived excitation temperature is much lower than what estimated from the CO lines in the g_1 component by (Lefloch et al. 2012) ($T_{ex} \sim 210$ K). This suggests that, similarly to what found for the other ions, the bulk of the observed SO^+ emission originates from the B1, B2 cavities.

To summarize, we estimate an SO^+ abundance of $\sim 8\ 10^{-10}$ in the outflow cavities. This value is 1–2 orders of magnitude larger than what predicted in cold clouds (Herbst & Leung 1986) and favor a shock origin, as suggested by previous detections of large SO^+ abundances in active star forming regions (Turner 1994). The chemistry of SO^+ is discussed in Sect. 5.

4.2.5. HCS^+

Fig. 2b shows the HCS^+ lines detected with the IRAM-30m telescope. HCS^+ has been previously detected in molecular clouds (e.g., Ohishi et al. 1992; Sutton et al. 1995), in the low-mass protostar IRAS 16293–2422 (e.g., Schöier et al. 2002), and in association with young sources driving outflows in Cepheus A (Codella et al. 2005). Emission in the bow-shock L1157-B1 was already reported by Bachiller & Perez Gutierrez (1997) and Yamaguchi et al. (2012). We detected the 2–1, 4–3, 5–4, and 6–5 lines with a signal-to-noise > 4, while only an upper limit is derived for the 7–6 line.

The signal to noise ratio is too low to perform a proper line profile analysis. No high velocity emission associated with the g_1 component is detected and the lines appear to be dominated by emission from the outflow cavity B1 (g_2). Additional emission by the old B2 cavity (g_3) could contribute close to systemic velocity.

Our LVG calculations confirm that the emission is dominated by the g_2 component. All the lines but the 2–1 are well reproduced by a single extended component with $T_{kin} \sim 80$ K, $n_{H_2} \sim 8\ 10^5$ cm^{-3}, and $N_{HCS^+} \sim 6\ 10^{11}$ cm^{-2}. The estimated physical conditions are consistent with those found for the B1 outflow cavity (i.e. the g_2 component), as derived from CO, and indicate an HCS^+ abundance of $7\ 10^{-10}$. However, the HCS^+ 2–1 observed line intensity is about twice as large as the one predicted by the LVG model for the g_2 component. In order to account for the intensity of the J=2–1, it is necessary to consider an additional component, of low excitation. Based on the HCS^+ 2–1 line profile this component could be associated with the B2 cavity, thus we assume the same physical conditions as derived from CO, i.e. $T_{kin} \sim 20$ K, $n_{H_2} \sim 10^5$ cm^{-3}. We find that for $N_{HCS^+} \sim 3\ 10^{11}$ cm^{-2} we obtain a good fit of the 2–1 line, while the contribution to the higher-J lines is negligible.

To summarize, we find that the HCS^+ profiles are well produced by the emission of the B1 and B2 outflow cavities, with similar abundances X_{HCS^+} of 7 and $3\ 10^{-10}$, respectively. These values are a factor four up to one order of magnitude lower than what estimated by Bachiller & Perez Gutierrez (1997) based on tentative detections of the 2–1, 5–4 lines. As for the other molecular ions, the chemistry of HCS^+ is discussed in Sect. 5.

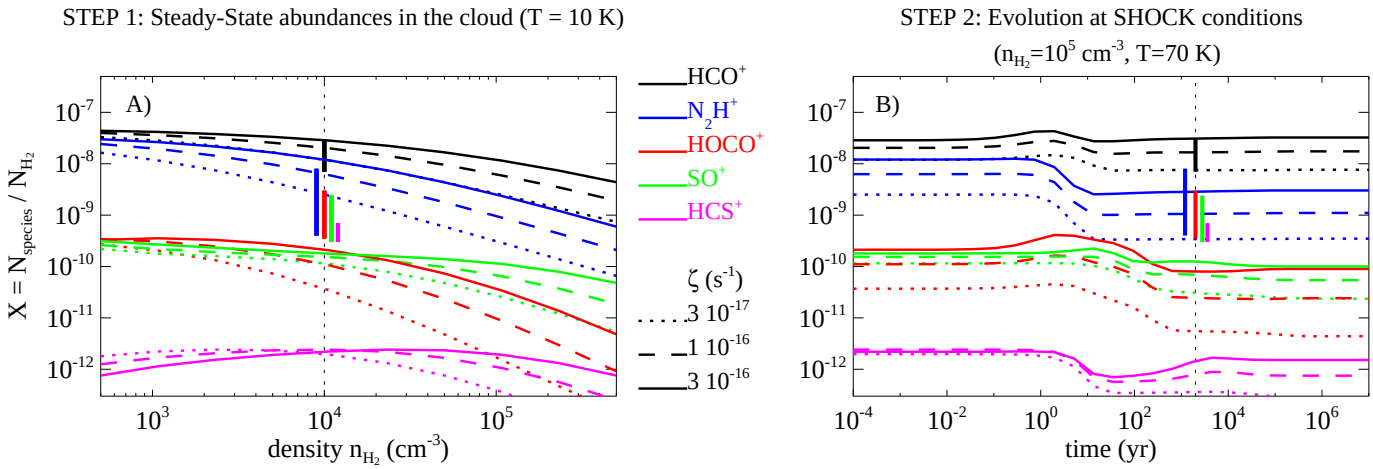

Fig. 4. Observed abundances of molecular ions (colour vertical bars) are compared with theoretical values calculated with Astrochem (colour lines). The colors indicate HCO^+ (black), N_2H^+(blue), $HOCO^+$ (red), SO^+ (green), and HCS^+ (magenta) abundances. *Panel A)* "STEP 1": steady-state abundances in the cloud, $X = N_{species}/N_{H_2}$, as a function of the gas density, n_{H_2} (cm^{-3}), for gas temperature T_{kin} = 10 K, and cosmic rays ionization rate ζ = 3 $10^{-17}, 10^{-16}, 3\ 10^{-16}$ s^{-1} (dotted, dashed, and solid lines). Observed abundances are overplot at the assumed cloud density (n_{H_2}= 10^4 cm^{-3}, vertical dotted line). *Panel B)* "STEP 2": evolution of steady-state abundances in the shock as a function of time (in years). The gas density and temperature are raised from cloud values (n_{H_2}= 10^4 cm^{-3}, T_{kin} = 10 K) to the observed values in the outflow cavity (n_{H_2}= 10^5 cm^{-3}, T_{kin} = 70 K). Observed abundances are overplot at the shock age (t_{shock} ~ 2000 years, vertical dotted line).

Table 3. Initial elemental abundances with respect to H_2 assumed in our chemical model.

Species	$X = N_{species}/N_{H_2}$
He	0.14
N	7.40 10^{-5}
O	3.52 10^{-4}
C^+	1.46 10^{-4}
S^+	1.60 10^{-7}
Si^+	1.60 10^{-8}
Fe^+	6.00 10^{-9}
Na^+	4.00 10^{-9}
Mg^+	1.40 10^{-8}

5. Chemistry of molecular ions

In order to understand the origin of the observed molecular ions we compare the abundances inferred from observations (see Table 2) with predictions obtained via the chemical code Astrochem[9]. Astrochem computes the chemical evolution of a gas at a given temperature, T_{kin}, and hydrogen density, n_H. The code reads a network of chemical reactions, builds a system of kinetic rates equations, and solves it using a state-of-the-art stiff ordinary differential equations (ODE) solver. It considers gas-phase processes and simple gas-grain interaction, such as freeze-out, and desorption via several mechanisms (thermal, cosmic-ray, and photo- desorption). In our calculations we use the OSU[10] chemical network, we assume visual extinction A_V = 10 mag consistent with $C^{18}O$ and ^{13}CO column densities, a grain size of 0.1 μm, and initial elemental abundances as assumed by Wakelam et al. (2006) in their low-metallicity model with the exception of He and N for which we assume cosmic abundances (e.g., Asplund et al. 2005; Tsamis et al. 2011) (see Table 3).

As a first step ("STEP 1"), we compute the evolution of the gas in the cloud before the passage of the shock, i.e. for a gas temperature T_{kin} = 10 K. Fig. 4A shows the steady-state abundances of the observed molecular ions for gas densities, n_{H_2}, between 5 10^2 and 5 10^5 cm^{-3}, and for three different values of the cosmic rays (CR) ionization rate (ζ = 3 $10^{-17}, 10^{-16}$, 3 10^{-16} s^{-1}). Note that the CR ionization rate in the interstellar medium varies between 10^{-17} to a few 10^{-16} s^{-1} (Padovani et al. 2009). Steady-state abundances are reached on a timescale of 10^6 – 10^7 years, i.e. much longer than the shock kinematical age (t_{shock} ~ 2000 years, Gueth et al. 1996). The abundances of HCO^+, N_2H^+, and $HOCO^+$ are enhanced by a factor of a few up to one order of magnitude for higher CR ionization rates, while they are decreased by 1 to 3 orders of magnitude with increasing density. The dependency of HCO^+, N_2H^+, and $HOCO^+$ abundance on ζ and n_{H_2} is due to the fact that in the quiescent gas the main formation process of these ions is via reactions with H_3^+:

$$H_3^+ + CO \rightarrow HCO^+ + H_2 \quad (1)$$

$$H_3^+ + N_2 \rightarrow N_2H^+ + H_2 \quad (2)$$

$$H_3^+ + CO_2 \rightarrow HOCO^+ + H_2 \quad (3)$$

where H_3^+ is produced by reaction of H_2 with H_2^+, which in turn is produced by cosmic ray ionization of H_2, and destructed by dissociative recombination with electrons. Hence the abundance of H_3^+ and, consequently, of these molecular ions increases with ζ and decreases with density. S-bearing species, SO^+ and HCS^+, are less dependent on the assumed ζ and stay roughly constant for densities up to 10^5 cm^{-3} if ζ = 1 – 3 10^{-16} s^{-1}.

As a second step ("STEP 2"), we compute how the obtained steady-state abundances evolve when the gas is compressed and heated in the shock, i.e. when density and temperature raise from typical dark cloud values (n_{H_2}= 10^4 cm^{-3}, T_{kin} = 10 K) to the observed values in the outflow cavity, g_2 (n_{H_2}= 10^5 cm^{-3}, T_{kin} = 70 K). Fig. 4B shows that molecular ions chemistry proceeds fast, so they adjust very rapidly to the change of physical conditions caused by the shock, on timescales shorter or comparable to the shock age (~ 2000 years). The abundance of all molecular ions drops due to the higher density but this is partially compensated for by the temperature enhancement.

[9] http://smaret.github.io/astrochem/
[10] http://www.physics.ohio-state.edu/ eric/research.html

Lastly, the evolution of molecular ions in the shock, i.e. "STEP 2", is re-calculated by enhancing (besides the gas temperature and density) the abundance of species which are thought to be sputtered off dust grain mantles, such as CO_2 and sulphur-bearing species (see Fig. 5). This is done by assuming ζ = 3 10^{-16} s^{-1}, which is the CR ionization value which best fit HCO^+ and N_2H^+ abundances (see below).

In the following, we discuss how the obtained steady-state abundances in the cloud and their evolution in the shock compare with observations for each of the detected molecular ions. In Fig. 4 and in Fig. 5 the observed abundances are shown as colour bars covering the range of values inferred for the different components, or, when only one abundance value is estimated, the relative uncertainty (see Sect. 4.2). Observations are overplot at the typical dark cloud density, n_{H_2}= 10^4 cm^{-3}, in Fig. 4A, and at the shock age, t_{shock} ~ 2000 years, in Figs. 4B and 5.

HCO^+ and N_2H^+ abundances:

Fig. 4A shows that the observed HCO^+ and N_2H^+ abundances are in agreement with what predicted in the quiescent gas in the cloud at n_{H_2}= 10^4 cm^{-3}, T_{kin} = 10 K. In the shock, the abundance of HCO^+ remains roughly constant, as the decrease due to compression is compensated for by the raise in temperature, while N_2H^+ decreases by a factor five up to one order of magnitude for the lowest CR ionization rate (Fig. 4B). Hence, HCO^+ and N_2H^+ observed abundances (X_{HCO^+} ~ 0.7 – 3 10^{-8}, $X_{N_2H^+}$ ~ 0.4 – 8 10^{-9}) are simultaneously reproduced at the shock age only by assuming a high CR ionization rate, i.e. ζ = 1 – 3 10^{-16} s^{-1}. Due to recombination, HCO^+ and N_2H^+ abundances are further decreased when neutral molecules are released off the dust grains. Thus, in the following we assume ζ = 3 10^{-16} s^{-1} to simultaneously fit the abundances of all the molecular ions (see below). The performed analysis indicates that, in agreement with what suggested by Codella et al. (2013), HCO^+ and N_2H^+ are not enhanced in the shock but instead are a fossil record of the pre-shock gas.

$HOCO^+$ abundance:

In contrast with HCO^+ and N_2H^+, the predicted $HOCO^+$ abundance in the cloud is lower than observed by a factor of a few up to two orders of magnitude depending on the assumed ζ (Fig. 4A). Moreover, the $HOCO^+$ abundance is further lowered following the gas compression in the shock, being one order of magnitude lower than observed even for the highest CR ionization rate ζ = 3 10^{-16} s^{-1} (Fig. 4B). As mentioned above, $HOCO^+$ is mainly formed via CO_2 reacting with H_3^+ (see Eq. 3), hence it may be a useful probe of CO_2, which lacks a permanent electric dipole moment making radio detection impossible. A low $HOCO^+$ abundance is expected in the cloud since most CO_2 is trapped on the icy dust mantles. In effect, we find that the steady-state abundance of CO_2 in the cloud (n_{H_2}= 10^4 cm^{-3}, T_{kin} = 10 K, ζ = 3 10^{-16} s^{-1}) is 3 10^{-7}, in agreement with what predicted by other chemical models (e.g., Lee et al. 1996) and what measured toward various star-forming regions through observations of the 15 μm band (van Dishoeck et al. 1996; Dartois et al. 1998; Boonman et al. 2003). Based on $HOCO^+$ observations in the Galactic center, Minh et al. (1991) first suggested that a high $HOCO^+$ abundance may be caused by shocks, which release CO_2 molecules frozen on the mantles of dust grains into gas-phase via grain-grain (shattering) or gas-grain (sputtering) collisions and/or via evaporation by UV-photons in dissociative shocks.

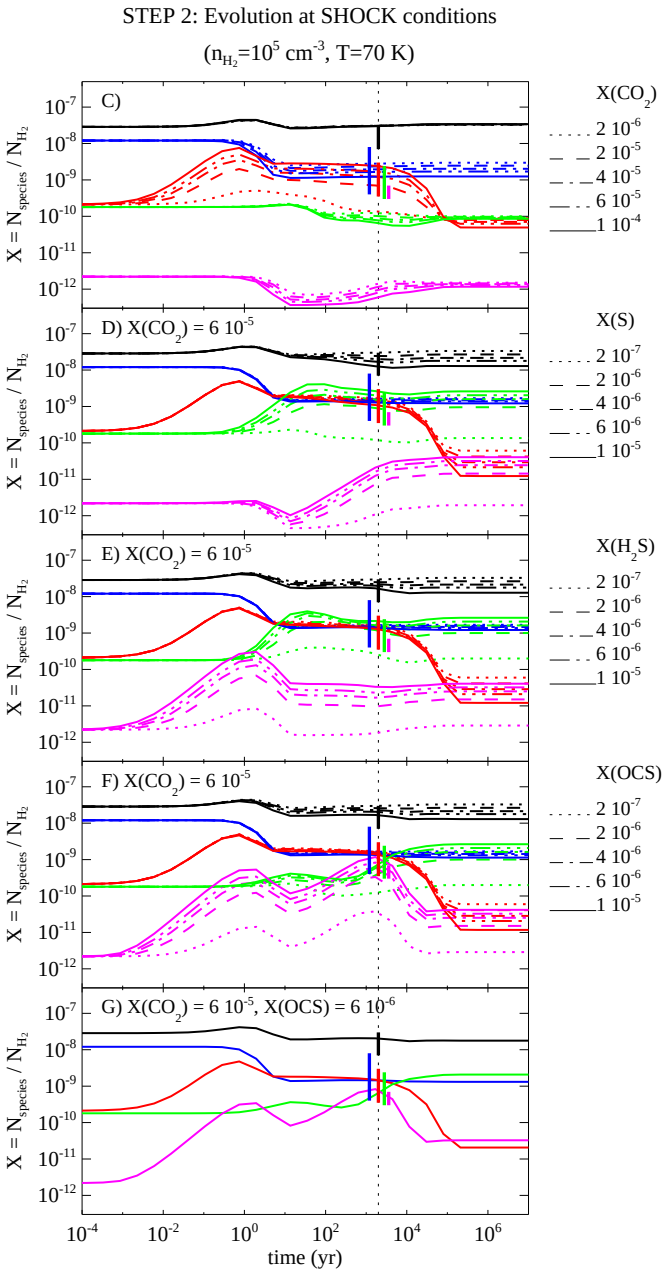

Fig. 5. Evolution of molecular ions abundances in the shock as a function of time ("STEP 2"). The colors indicate HCO^+ (black), N_2H^+(blue), $HOCO^+$ (red), SO^+ (green), and HCS^+ (magenta) abundances. Observed abundances (colour vertical bars) are overplot at the shock age (t_{shock} ~ 2000 years, vertical dotted line). The evolution is computed from steady-state values in the cloud (n_{H_2}= 10^4 cm^{-3}, T_{kin} = 10 K, ζ = 3 10^{-16} s^{-1}) by enhancing the gas temperature and density (n_{H_2}= 10^5 cm^{-3}, T_{kin} = 70 K), and the abundance of molecules which are thought to be sputtered off dust grain mantles: CO_2, S, H_2S, and OCS (*panels C), D), E), and F)*, respectively). When varying S, H_2S, and OCS abundances, X_{CO_2} is set to = 6 10^{-5}. Finally, *panel G)* shows the evolution of molecular ions abundances in our "best-fit model", i.e. for X_{CO_2} = 6 10^{-5} and X_{OCS} = 6 10^{-6}.

We investigate this scenario with Astrochem by computing the evolution of $HOCO^+$ in the shock when enhancing CO_2 with respect to its steady-state abundance. Note that we have direct evidence of dust grains sputtering in the B1 shock from

SiO observations (Gueth et al. 1998; Nisini et al. 2007). Fig. 5C shows that $HOCO^+$ is rapidly enhanced by more than one order of magnitude for increasing X_{CO_2} and it stays high for $\sim 10^4$ years. The observed value, $X_{HOCO^+} \sim 10^{-9}$, is matched at the shock age ($t_{shock} \sim 2000$ years) for $X_{CO_2} \geq 2\ 10^{-5}$, i.e. around two orders of magnitude larger than in the cloud. This value is consistent with previous estimates of the amount of solid CO_2 trapped into the icy mantle of dust grains (e.g., D'Hendecourt & Jourdain de Muizon 1989; Tielens et al. 1991; de Graauw et al. 1996). Thus, this result may indicate total evaporation of the ice mantles, in agreement with the water abundance estimated by Busquet et al. (2013) in the hot shock component.

The abundance of the other molecular ions is not (for HCO^+) or only slightly (by a factor lower than two for the other molecular ions) affected by the CO_2 enhancement in the shock.

SO^+ abundance:

In agreement with what estimated by previous gas-phase chemistry models (e.g., Herbst & Leung 1986), our chemical model predicts an SO^+ steady-state abundance in the cloud of $1.8\ 10^{-10}$, which is lowered down to $1\ 10^{-10}$ in the shock. This is lower than observed by around one order of magnitude. On the other hand, Neufeld & Dalgarno (1989) have shown that the abundance of SO^+ is strongly enhanced in shocks due to the release of sulphur from dust mantles and its subsequent ionization, as SO^+ is primarily formed via $S^+ + OH \rightarrow SO^+ + H$.

We explore this scenario by computing the evolution of molecular ions in the shock when enhancing the abundance of atomic S or H_2S (Figs. 5D and 5E, respectively). Note that S and H_2S are enhanced up to values which are larger than the initial abundance of S^+ in the model, as most of S is assumed to be trapped onto dust grains initially. However, they are still consistent with the solar abundance of S (e.g., Asplund et al. 2005). Following our analysis of $HOCO^+$ we also set $X_{CO_2} = 6\ 10^{-5}$. Fig. 5 shows that, if the released S or H_2S are $\sim 2\ 10^{-6}$ and $\geq 2\ 10^{-7}$ respectively, SO^+ is rapidly (less than 10 years) enhanced behind the shock and its abundance remains high over large timescales, matching the observed value ($X_{SO^+} \sim 8\ 10^{-10}$) at the shock age. This confirms a shock origin for SO^+.

Note that the amount of H_2S which needs to be released in gas-phase to reproduce the observed SO^+ abundance is in agreement with the H_2S abundance in the B1 shock estimated by Bachiller & Perez Gutierrez (1997) ($X_{H_2S} \sim 3\ 10^{-7}$).

Concerning the other molecular ions we note that the abundances of N_2H^+ and $HOCO^+$ are poorly affected by S or H_2S enhancement, while the abundance of HCO^+ is lowered by a factor lower than two, still matching the observed value. HCS^+ is also enhanced but not enough to match the observed abundance (see below).

HCS^+ abundance:

Fig. 4 shows that the HCS^+ abundance in the cloud is very low $\sim 10^{-12}$, even for high CR ionization rates, and it remains roughly unaltered after the passage of the shock. The abundance of HCS^+ is strongly related to that of CS, as this ion is formed when CS reacts with HCO^+, H_3^+, and H_3O^+, while the main destructive mechanism is dissociative recombination into CS. Hence, the low values of X_{HCS^+} in the cloud are likely due to a lack of CS. Indeed, the steady-state abundance of CS in the cloud ($n_{H_2} = 10^4$ cm^{-3}, $T_{kin} = 10$ K, $\zeta = 3\ 10^{-16}$ s^{-1}) is of $\sim 10^{-10}$, which is three orders of magnitude lower than what estimated in the B1 shock by Bachiller & Perez Gutierrez (1997) ($X_{CS} \sim 2\ 10^{-7}$).

Figs. 5D and 5E show that HCS^+ is enhanced by almost two orders of magnitude when S or H_2S are released off the dust grains but is still lower than observed by one order of magnitude. However, larger CS and HCS^+ abundances can be obtained if we assume that OCS is one of the main sulphur carrier on dust grains, as suggested by Wakelam et al. (2004, 2005) and Codella et al. (2005). In particular, Fig. 5F shows that the observed HCS^+ abundance ($X_{HCS^+} \sim 3 - 7\ 10^{-10}$) is matched at the shock age when the abundance of OCS in the shock is enhanced up to values $\geq 2\ 10^{-6}$. Interestingly, also X_{CS} turns out to be in agreement with the observed value within a factor two ($X_{CS} \sim 2\ 10^{-7}$, Bachiller & Perez Gutierrez 1997).

On the other hand we note that if the amount of OCS released off the dust grains is $\geq 2\ 10^{-6}$ the OCS abundance at the shock age is $\sim 10^{-6}$, and it decreases down to value of $\sim 10^{-7}$ only on timescales $\geq 10^4$ years. Thus, X_{OCS} at the shock age is around 1–2 orders of magnitude larger than what estimated in the B1–B2 cavities by Bachiller & Perez Gutierrez (1997) ($X_{OCS} \sim 3\ 10^{-8} - 2\ 10^{-7}$). In this regard, several authors point out that at present chemical models are unable to explain simultaneously CS, HCS^+, and OCS abundances and that the chemistry of sulphur-bearing species is not fully understood (Doty et al. 2004; Wakelam et al. 2004, 2005). Doty et al. (2004) note that the rates of ion-molecule reaction producing HCS^+, i.e. (HCO^+, H_3^+, H_3O^+) + CS, have been only estimated but would need to be confirmed by laboratory experiments.

"Best-fit model":

Fig. 5 shows that the abundances of the detected molecular ions (see Tab. 2) are well reproduced by the gas evolution in the shock if CO_2, S, and OCS are substantially enhanced due to dust grains sputtering and/or evaporation. In particular, we are able to simultaneously match all the estimated abundances at the shock age (~ 2000 years) if we assume $X_{CO_2} = 6\ 10^{-5}$ and $X_{OCS} = 6\ 10^{-6}$ (see Fig. 5G). In order to verify the robustness of our "best-fit model", we verify that the abundances of other species, both ionic and neutral, are consistent with present and past observations. The abundances obtained at the shock age of molecular ions and anions which are not-detected in our survey are summarized in Tab. 4. Note that they are all $< 10^{-10}$, hence consistent with non-detection of the transitions falling in the spectral range covered by our survey, with the exception of H_3O^+, whose predicted abundance is $8\ 10^{-9}$. The only H_3O^+ transition covered by our survey is the transition at 307.2 GHz, observed with WILMA with a resolution of 2 MHz, for which we derive an upper limit of 0.03 K km s^{-1}. This is consistent with non-detection when assuming the gas temperature and density inferred for the g_2 component.

6. Conclusions

In this paper we presented a comprehensive study of the chemistry of molecular ions in protostellar shocks. As part of the ASAI and CHESS projects, we performed a census of molecular ions in the chemically rich protostellar shock L1157-B1 by means of an unbiased and high sensitivity (~ 1.5 mK in the 3 mm band) spectral survey executed with the IRAM-30m telescope and *Herschel*/HIFI. From our analysis we obtained the following results:

- we report emission from HCO^+, N_2H^+, HCS^+ and, for the first time in a protostellar shock, from $HOCO^+$ and SO^+.

Table 4. Abundances of non-detected molecular ions with respect to H_2, as obtained from our "best-fit model" (see Fig. 5G).

Species	$X = N_{species}/N_{H_2}$
CO^+	$6\ 10^{-14}$
H_2O^+	$7\ 10^{-13}$
H_3O^+	$8\ 10^{-9}$
CH^+	$6\ 10^{-16}$
HOC^+	$1\ 10^{-11}$
$HCNH^+$	$4\ 10^{-11}$
NH_4^+	$9\ 10^{-11}$
CN^-	$2\ 10^{-18}$
C_3N^-	$3\ 10^{-18}$
C_4H^-	$1\ 10^{-16}$

- all the detected lines peak at blueshifted velocity, $\sim 0.5-3$ km s^{-1} with respect to systemic (V_{sys} = +2.6 km s^{-1}), and have a line width of $\sim 3-7$ km s^{-1}. A higher velocity component (V up to -40 km s^{-1}) associated with the primary jet is detected in the HCO^+ 1–0 line.

- the lines profiles can be decomposed into different velocity components following an exponential intensity-velocity relation as found for the CO lines (Lefloch et al. 2012). The bulk of the emission is associated with the extended outflow cavities and originates from a gas with temperature $T_{kin} \sim 20-70$ K, and density $n_{H_2} \sim 10^5$ cm^{-3}, in agreement with what found for the CO lines.

- inferred HCO^+ and N_2H^+ abundances ($X_{HCO^+} \sim 0.7-3\ 10^{-8}$, $X_{N_2H^+} \sim 0.4-8\ 10^{-9}$) are in agreement with on-source values (Bachiller & Perez Gutierrez 1997), suggesting that these species are not enhanced in the shock. This is further confirmed by the fact that the observed abundances are in agreement with steady-state abundances in the cloud (i.e. at T_{kin} = 10 K, $n_{H_2} = 10^4$ cm^{-3}). The decrease of their abundance due to gas compression in the shock is compensated for by the raise in temperature, and predicted values match the observations for high cosmic rays ionization rate $\zeta = 3\ 10^{-16}$ s^{-1}. Hence, HCO^+ and N_2H^+ are a fossil-record of the gas chemistry before the arrival of the shock.

- $HOCO^+$, SO^+, and HCS^+ abundances ($X_{HOCO^+} \sim 10^{-9}$, $X_{SO^+} \sim 8\ 10^{-10}$, $X_{HCS^+} \sim 3-7\ 10^{-10}$), instead, are 1–2 orders of magnitude larger than predicted steady-state abundances in the cloud. On the other hand, they are strongly enhanced in the shock if CO_2, S, H_2S, and OCS abundances are increased with respect to steady-state due to release off the dust grains in the shock. Hence, as suggested by previous studies (e.g. Minh et al. 1991; Deguchi et al. 2006; Turner 1992, 1994), these species are effective shock tracers.

- the observed abundances allow constraining the amount of CO_2 and sulphur-bearing species released in the shock. To reproduce $HOCO^+$ observations, CO_2 should be enhanced up to abundances $\geq 2\ 10^{-5}$, i.e. two order of magnitude larger than its gas-phase abundance in the quiescent gas. This is in agreement with previous estimate of the CO_2 content on dust mantles. To reproduce SO^+, instead, the sulphur released in the form of H_2S molecules should be $\geq 2\ 10^{-7}$. This value is in agreement with the H_2S abundance in B1 estimated by Bachiller & Perez Gutierrez (1997).

- as noted in previous studies, CS and HCS^+ abundances in the quiescent gas in dark clouds are very low. However, the observed HCS^+ and CS abundances ($X_{HCS^+} \sim 3-7\ 10^{-10}$, $X_{CS} \sim 2\ 10^{-7}$) are matched if OCS is assumed to be one of the main sulphur career on dust grains, as suggested by Wakelam et al. (2004, 2005) and Codella et al. (2005). Hence its abundance is enhanced to values $\geq 2\ 10^{-6}$ in the shock. Such high X_{OCS} values, however, are at least one order of magnitude larger than estimated by Bachiller & Perez Gutierrez (1997) and are lowered to the observed values only on timescales $\geq 10^4$ years, i.e. much larger than the shock age ($t_{shock} \sim 2000$ years). This difficulty in simultaneously reproducing CS, HCS^+, and OCS abundances was already reported by other authors and indicates that the chemistry of sulphur-bearing species is not yet fully understood (Doty et al. 2004; Wakelam et al. 2004, 2005). In this regard, laboratory experiments are required to verify the rates of ion-molecule reaction producing HCS^+, i.e. (HCO^+, H_3^+, H_3O^+) + CS.

Acknowledgements. L. Podio acknowledges the funding from the FP7 Intra-European Marie Curie Fellowship (PIEF-GA-2009-253896). B. Lefloch and C. Ceccarelli acknowledge the financial support by the French space agency CNES. R. Bachiller acknowledges partial support from Spanish MINECO under grant FIS2012-32096.

References

Asplund, M., Grevesse, N., & Sauval, A. J. 2005, in Astronomical Society of the Pacific Conference Series, Vol. 336, Cosmic Abundances as Records of Stellar Evolution and Nucleosynthesis, ed. T. G. Barnes, III & F. N. Bash, 25
Bachiller, R. & Perez Gutierrez, M. 1997, ApJ, 487, L93
Bachiller, R., Pérez Gutiérrez, M., Kumar, M. S. N., & Tafalla, M. 2001, A&A, 372, 899
Benedettini, M., Busquet, G., Lefloch, B., et al. 2012, A&A, 539, L3
Benedettini, M., Viti, S., Codella, C., et al. 2007, MNRAS, 381, 1127
Benedettini, M., Viti, S., Codella, C., et al. 2013, MNRAS
Boonman, A. M. S., van Dishoeck, E. F., Lahuis, F., & Doty, S. D. 2003, A&A, 399, 1063
Busquet, G., Lefloch, B., Benedettini, M., et al. 2013, ArXiv e-prints
Caselli, P., Benson, P. J., Myers, P. C., & Tafalla, M. 2002, ApJ, 572, 238
Caselli, P., Walmsley, C. M., Terzieva, R., & Herbst, E. 1998, ApJ, 499, 234
Ceccarelli, C. & CHESS Consortium. 2010, in COSPAR Meeting, Vol. 38, 38th COSPAR Scientific Assembly, 2476
Codella, C., Bachiller, R., Benedettini, M., et al. 2005, MNRAS, 361, 244
Codella, C., Benedettini, M., Beltrán, M. T., et al. 2009, A&A, 507, L25
Codella, C., Ceccarelli, C., Bottinelli, S., et al. 2012a, ApJ, 744, 164
Codella, C., Ceccarelli, C., Lefloch, B., et al. 2012b, ApJ, 757, L9
Codella, C., Lefloch, B., Ceccarelli, C., et al. 2010, A&A, 518, L112
Codella, C., Viti, S., Ceccarelli, C., et al. 2013, ArXiv e-prints
Dartois, E., D'Hendecourt, L., Boulanger, F., et al. 1998, A&A, 331, 651
Davis, C. J. & Eisloeffel, J. 1995, A&A, 300, 851
de Graauw, T., Helmich, F. P., Phillips, T. G., et al. 2010, A&A, 518, L6
de Graauw, T., Whittet, D. C. B., Gerakines, P. A., et al. 1996, A&A, 315, L345
Deguchi, S., Miyazaki, A., & Minh, Y. C. 2006, PASJ, 58, 979
D'Hendecourt, L. B. & Jourdain de Muizon, M. 1989, A&A, 223, L5
Doty, S. D., Schöier, F. L., & van Dishoeck, E. F. 2004, A&A, 418, 1021
Dubernet, M.-L., Alexander, M. H., Ba, Y. A., et al. 2013, A&A, 553, A50
Flower, D. R. 1999, MNRAS, 305, 651
Girart, J. M., Ho, P. T. P., Rudolph, A. L., et al. 1999, ApJ, 522, 921
Girart, J. M., Viti, S., Williams, D. A., Estalella, R., & Ho, P. T. P. 2002, A&A, 388, 1004
Gueth, F., Guilloteau, S., & Bachiller, R. 1996, A&A, 307, 891
Gueth, F., Guilloteau, S., & Bachiller, R. 1998, A&A, 333, 287
Hammami, K., Lique, F., Jaïdane, N., et al. 2007, A&A, 462, 789
Herbst, E., Green, S., Thaddeus, P., & Klemperer, W. 1977, ApJ, 215, 503
Herbst, E. & Leung, C. M. 1986, MNRAS, 222, 689
Hogerheijde, M. R., van Dishoeck, E. F., Blake, G. A., & van Langevelde, H. J. 1998, ApJ, 502, 315
Lee, C.-F., Ho, P. T. P., Hirano, N., et al. 2007, ApJ, 659, 499
Lee, H.-H., Bettens, R. P. A., & Herbst, E. 1996, A&AS, 119, 111
Lefloch, B., Cabrit, S., Busquet, G., et al. 2012, ApJ, 757, L25

Lefloch, B., Cabrit, S., Codella, C., et al. 2010, A&A, 518, L113
Looney, L. W., Tobin, J. J., & Kwon, W. 2007, ApJ, 670, L131
Minh, Y. C., Brewer, M. K., Irvine, W. M., Friberg, P., & Johansson, L. E. B. 1991, A&A, 244, 470
Minh, Y. C., Irvine, W. M., & Ziurys, L. M. 1988, ApJ, 334, 175
Monteiro, T. 1984, MNRAS, 210, 1
Müller, H. S. P., Thorwirth, S., Roth, D. A., & Winnewisser, G. 2001, A&A, 370, L49
Neufeld, D. A. & Dalgarno, A. 1989, ApJ, 340, 869
Nisini, B., Benedettini, M., Codella, C., et al. 2010, A&A, 518, L120
Nisini, B., Codella, C., Giannini, T., et al. 2007, A&A, 462, 163
Ohishi, M., Irvine, W. M., & Kaifu, N. 1992, in IAU Symposium, Vol. 150, Astrochemistry of Cosmic Phenomena, ed. P. D. Singh, 171
Padovani, M., Walmsley, C. M., Tafalla, M., Galli, D., & Müller, H. S. P. 2009, A&A, 505, 1199
Pickett, H. M., Poynter, R. L., Cohen, E. A., et al. 1998, J. Quant. Spec. Radiat. Transf., 60, 883
Pilbratt, G. L., Riedinger, J. R., Passvogel, T., et al. 2010, A&A, 518, L1
Rawlings, J. M. C., Redman, M. P., Keto, E., & Williams, D. A. 2004, MNRAS, 351, 1054
Roelfsema, P. R., Helmich, F. P., Teyssier, D., et al. 2012, A&A, 537, A17
Sakai, N., Sakai, T., Aikawa, Y., & Yamamoto, S. 2008, ApJ, 675, L89
Schöier, F. L., Jørgensen, J. K., van Dishoeck, E. F., & Blake, G. A. 2002, A&A, 390, 1001
Sutton, E. C., Peng, R., Danchi, W. C., et al. 1995, ApJS, 97, 455
Tafalla, M. & Bachiller, R. 1995, ApJ, 443, L37
Tafalla, M., Santiago-García, J., Hacar, A., & Bachiller, R. 2010, A&A, 522, A91
Tappe, A., Forbrich, J., Martín, S., Yuan, Y., & Lada, C. J. 2012, ApJ, 751, 9
Thaddeus, P., Guelin, M., & Linke, R. A. 1981, ApJ, 246, L41
Tielens, A. G. G. M., Tokunaga, A. T., Geballe, T. R., & Baas, F. 1991, ApJ, 381, 181
Tsamis, Y. G., Walsh, J. R., Vílchez, J. M., & Péquignot, D. 2011, MNRAS, 412, 1367
Turner, B. E. 1992, ApJ, 396, L107
Turner, B. E. 1994, ApJ, 430, 727
Turner, B. E. 1996, ApJ, 468, 694
Turner, B. E., Terzieva, R., & Herbst, E. 1999, ApJ, 518, 699
van Dishoeck, E. F., Helmich, F. P., de Graauw, T., et al. 1996, A&A, 315, L349
Vasta, M., Codella, C., Lorenzani, A., et al. 2012, A&A, 537, A98
Viti, S., Natarajan, S., & Williams, D. A. 2002, MNRAS, 336, 797
Wakelam, V., Caselli, P., Ceccarelli, C., Herbst, E., & Castets, A. 2004, A&A, 422, 159
Wakelam, V., Ceccarelli, C., Castets, A., et al. 2005, A&A, 437, 149
Wakelam, V., Herbst, E., Selsis, F., & Massacrier, G. 2006, A&A, 459, 813
Wilson, T. L. & Rood, R. 1994, ARA&A, 32, 191
Yamaguchi, T., Takano, S., Watanabe, Y., et al. 2012, PASJ, 64, 105